# Structural relaxation of amorphous $Pd_{82}Si_{18}$: X-ray measurements, electrical-resistivity measurements, and a comparison using the Ziman theory

E. Chason, A. L. Greer,* K. F. Kelton,† P. S. Pershan, L. B. Sorensen,‡ F. Spaepen, and A. H. Weiss§
*Division of Applied Sciences, Harvard University, 29 Oxford Street, Cambridge, Massachusetts 02138*
(Received 28 January 1985)

Structural relaxation in amorphous $Pd_{82}Si_{18}$ is studied using high-precision x-ray diffraction. The x-ray structure factor $S(k)$ and the density $\rho$ (determined from the x-ray absorption), are measured simultaneously as a function of the annealing conditions. The measured changes in $S(k)$ are compared with those expected from simple densification using a Percus-Yevick model with two hard-sphere diameters. The variation in the electrical resistivity with annealing is also measured and is compared with the resistivity change estimated from the x-ray measurements using the Ziman theory. To allow a direct comparison of the x-ray and electrical measurements, we derive an approximate relationship between the x-ray atomic scattering factor and the pseudopotential as a substitute for a first-principles calculation. The combination of the low scattering rate from the amorphous samples and the high precision ($<0.1\%$) necessary to allow direct comparison requires special techniques to maintain adequate system stability.

## I. INTRODUCTION

Amorphous metals are characterized by an atomic structure lacking long-range translational order.[1] As a result of rapid quenching of a liquid alloy in which crystal nucleation or growth can be avoided, the disordered liquidlike structure is frozen in, in the sense that at room temperature it is unable to change on an experimental time scale. Annealing the as-quenched material at a temperature where rapid crystallization is kinetically inhibited allows a relaxation to a more stable amorphous structure. This structural relaxation process results in a continuous change in all the physical properties.[2] The change in the structure factor $S(k)$ can be measured directly with x-ray scattering, and this change can then be related to the changes in the other physical properties of the material.

Although there have been many measurements of the structure factor in amorphous metals, there have been few careful measurements of the change in $S(k)$ associated with structural relaxation. The aim of this work is twofold: (i) to make a precise measurement of the change in $S(k)$ with structural relaxation for comparison with the Percus-Yevick hard-sphere model[3] using measured changes in the density to predict changes in $S(k)$ and (ii) to assess the validity of the Ziman theory[4] by making a quantitative comparison between measured changes in the electrical resistivity and those calculated from the changes in the structure factor $S(k)$. By measuring changes in the resistivity rather than the absolute resistivity, we concentrate on the part of the Ziman theory that is structure dependent, and less on the pseudopotential which is relatively independent of the structure. Previous comparisons of Ziman theory calculations with experiment for the absolute resistivity are more sensitive to the calculation of the pseudopotential.[5]

To accomplish this, changes upon annealing in both the density $\rho$ and the structure factor $S(k)$ of "splat-quenched" $Pd_{82}Si_{18}$ were simultaneously measured from the x-ray absorption and the x-ray scattering. Estimates of the change in the resistivity, obtained from the Ziman theory for the measured changes in $S(k)$ and $\rho$, are compared with direct measurements of the change in the resistivity. This comparison serves as a test of the applicability of the Ziman theory in metal-metalloid alloys where $d$-band effects are negligible.[5]

In Sec. II we describe the apparatus and the technical difficulties involved in making the required high precision x-ray measurements on amorphous metals. Also included is a discussion of the stability of the spectrometer and the special difference technique we developed to reduce the drifts in the system to the required levels by using two samples, one which was annealed and one which served as a standard. The section on densification (Sec. III) describes how the changes in the sample density are calculated from the changes in the measured x-ray transmission after each anneal. The corrections to the data for normalization, absorption, air scattering and polarization are discussed in the data analysis section (Sec. IV), and the resulting scattering intensities in electron units are presented. In Sec. V, the scattering intensity is related to a simple two-component hard-sphere model and qualitative agreement between the data and the model is demonstrated. The final section reviews the Ziman theory and describes a simple approximation that allows us to calculate the resistivity from the x-ray scattering without calculating the atomic pseudopotential. Finally, the Ziman theory results are compared with the resistivity measurements made on the same samples.

## II. EXPERIMENT

Changes in the x-ray structure factor and the electrical resistivity were measured at room temperature as a function of isothermal annealing time. The samples were produced by splat quenching, resulting in thin discs approximately 2 cm in diameter and 50 $\mu$m thick. Each x-ray

 

TABLE I. Summary of results.

| Annealing temperature (°C) | Annealing time (min) | Densification (%) | $R_a$ (%) | $R_t$ (%) | Change in peaks heights (%) | Second moment (Å$^{-1}$) | Centroid (Å$^{-1}$) | Change in $2k_F$ (Å$^{-1}$) | Change in electrical resistivity from Ziman theory (%) |
|---|---|---|---|---|---|---|---|---|---|
| 266 | 0 | 0 | 94.259±0.020 | 79.370±0.033 | 0 | 0.315 88 | 2.875 60±0.000 24 | 0 | 0 |
| 266 | 40 | 0.223±0.044 | 94.193±0.016 | 79.182±0.015 | 0.96(±0.05) | 0.314 70 | 2.875 96±0.000 11 | 0.0018±0.0004 | −0.37±0.16 |
| 266 | 160 | 0.256±0.056 | 94.178±0.021 | 79.155±0.018 | 1.08 | 0.314 60 | 2.875 93±0.000 19 | 0.0021±0.0004 | −0.37±0.16 |
| 266 | 300 | 0.263±0.048 | 94.105±0.027 | 79.148±0.021 | 1.15 | 0.314 44 | 2.875 82±0.000 17 | 0.0021±0.0004 | −0.51±0.16 |
| 241 | 0 | 0 | 103.019±0.033 | 105.570±0.024 | 0 | 0.314 51 | 2.875 44±0.000 18 | 0 | 0 |
| 241 | 15 | 0.118±0.042 | 102.897±0.035 | 105.469±0.022 | 0.19 | 0.313 87 | 2.875 56±0.000 20 | 0.0010±0.0003 | −0.37±0.16 |
| 241 | 60 | 0.262±0.062 | 102.703±0.026 | 105.359±0.018 | 0.37 | 0.313 70 | 2.875 16±0.000 19[a] | 0.0021±0.0004 | −0.33±0.16 |
| 241 | 360 | 0.407±0.065 | 102.665±0.050 | 105.231±0.019 | 0.72 | 0.313 44 | 2.875 15±0.000 14 | 0.0033±0.0004 | −0.19±0.16 |

[a]Centroid of scans taken after beam motion.

sample was taken from the center of a disc and the corresponding resistivity sample was cut from the adjacent material, ensuring identical starting materials.

The electrical resistivity was measured with a four-point probe ac bridge technique, using a lock-in amplifier, following the method reported earlier.[6] The measured resistances were corrected for the sample densification to obtain the resistivity changes.

For the x-ray measurements, a series of four anneals was performed on two separate samples at different temperatures (see Table I). The anneals were performed in a vacuum furnace constructed with aluminum heater blocks that ensured a uniform temperature distribution across the sample. The temperature gradient, measured with a set of thermocouples, was less than 2 °C along the sample. The time to heat from 180 °C (below which no measurable changes in resistivity occur) to the annealing temperature was approximately two minutes. During the anneals, the furnace was backfilled with nitrogen to increase the thermal contact between the sample and the heater; at the end of the anneal, it was flushed with fresh nitrogen to cool the sample quickly.

The apparatus used for the x-ray measurements is shown schematically in Fig. 1. A Rigaku RU-200 rotating anode generator, operating at 8 kW with a molybdenum anode was used to produce high-intensity radiation. The [002] reflection from a flat graphite monochromator was used to select the MoK$\alpha$ radiation wavelength ($\lambda = 0.7107$ Å) and to collimate the beam. Horizontal and vertical slits after the monochromator determined the beam size and rejected most of the bremsstrahlung. The incident beam monitor, mounted between the exit slit of the monochromator and the sample, consisted of a 5-mil thick Kapton foil that scattered approximately $10^{-5}$ of the beam 90° into an NaI scintillation detector. An identical monitor was placed behind the sample to measure the sample absorption. The changes in the absorptivity with annealing were used to calculate the sample densification. The angular acceptance of the transmitted beam monitor was approximately 4° in the horizontal and vertical direction, so all the small angle scattering was accepted. Previous measurements of the small angle scattering from $Pd_{82}Si_{18}$ (Ref. 7) as a function of annealing confirm that the change in the small angle scattering is very small and confined to this region. A receiving slit followed by a second [002] graphite analyzer and a third NaI detector mounted on the $2\theta$ arm were used to measure the elastically scattered radiation. The angular resolution was measured to be 0.65° full width at half maximum at zero arm.[8]

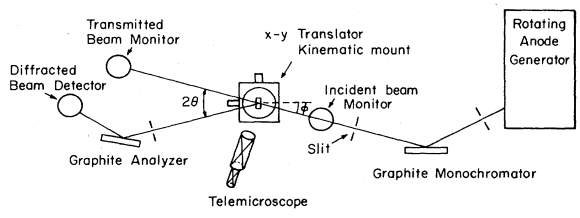


FIG. 1. Schematic diagram of the x-ray spectrometer.

The graphite crystals were $1\times1$ in.$^2$ The monochromator was positioned 30 cm from the x-ray source; the effective source size was $0.5\times1$ mm$^2$. The monochromator exit slit was 33 cm from the monochromator and was set at 3 mm wide$\times$9 mm high. Vacuum flight paths were used between the source and the monochromator exit slits, except for 6 cm on either side of the monochromator. The sample was 20 cm from the monochromator exit slit. The analyzer slits on the $2\theta$ arm were 39 cm from the sample and were set at a width of 2.05 mm and a height of 10 mm. The analyzer crystal was 10 cm behind the slits. The spectrometer used a Huber two-circle goniometer with independent sample angle $\phi$ and scattering angle $2\theta$, which was controlled by a PDP 11/34 minicomputer interfaced through a CAMAC crate.

The x-ray diffraction measurements were performed in the transmission geometry. At the angles of interest, a much smaller portion of the sample was illuminated in the transmission geometry than in the reflection geometry; this minimized the possible effects due to sample inhomogeneity. The scattering angle ($2\theta$) was maintained at twice the sample angle ($\phi$) so that the absorption correction is particularly simple.[9] Each scan covered the first peak in the structure factor; the scattering vector $k=(4\pi/\lambda)\sin(\theta)$, was scanned from 2.0 to 3.8 Å$^{-1}$ in constant steps of 0.015 Å$^{-1}$. Each point in the scan was measured for $5\times10^5$ monitor counts which took approximately 26 s; an entire scan took approximately 1 h. Multiple scans were collected between each anneal.

The precision required for the x-ray measurement was estimated from the measured changes in the electrical resistivity[6] to be 0.1%. The minimum percent error was determined by Poisson statistics; $\sigma(\%)=1/\sqrt{N}$, where $N$ is the number of photons counted. At $k=2.42$ Å$^{-1}$, the region of particular interest as explained below, the count rate was 1350 counts/s, so 27 scans per anneal were necessary to reduce the counting noise below 0.1%. Since four anneals were performed per sample, the systematic errors had to be kept below 0.1% over a 100-h period.

The required long counting times imposed stringent conditions on the mechanical stability of the spectrometer. The x-ray beam position, beam intensity, and sample position had to be carefully monitored. At a typical scattering angle of 20°, it was determined experimentally that sample motion greater than 20 $\mu$m parallel to the beam or a beam motion of 0.001° gave minimum intensity errors greater than 0.1%. This was partly due to the finite size of the graphite analyzer ($1\times1$ in.$^2$); it was not sufficiently wide to accept all of the scattered radiation that fell within its angular acceptance range. As a result, the crystal acted as an effective slit even when the analyzer slits were fully open. The resulting sensitivity to sample motion was reduced as much as possible by proper alignment of the analyzer slits with respect to the crystal. The sample was translated by an $x$-$y$ positioner to measure the effect of sample motion on the integrated peak intensity for different slit positions. The slits were then set to minimize the sensitivity to sample motion. In this position the resolution function of the crystal and the analyzer slit were coincident. Using this procedure, the integrated peak intensity changed only to second order as a function of the displacement of the sample away from the center of the goniometer.

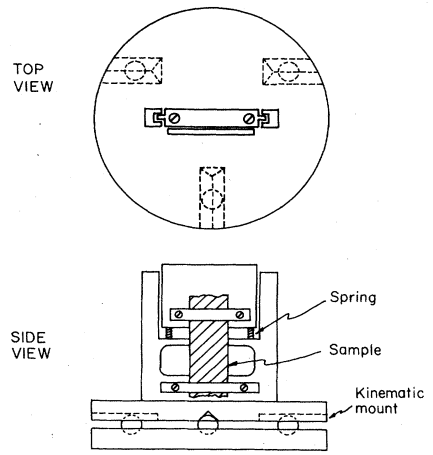


FIG. 2. Spring-loaded sample holder for $Pd_{82}Si_{18}$ samples. The kinematic mount allowed the sample to be removed and to then be repositioned to within $\pm10$ $\mu$m.

The sample holder was designed to minimize sample motion during the anneal. As shown in Fig. 2, the sample holder was constructed on a kinematic mount which allowed it to be removed and to be placed in the vacuum furnace for the anneals and to then be replaced on the x-ray spectrometer within 10 $\mu$m of its original position. The kinematic mount consisted of a base with three ball bearings set in it, attached to the goniometer. Grooves on the underside of the sample holder fit securely on the ball bearings at only one position. The sample position was checked by a telemicroscope after each anneal. Samples were held in a spring loaded slide which accommodated the strains that otherwise would have developed during the thermal treatments. Previous measurements of the changes in the x-ray structure factor[10] used samples that were spot-welded to a stainless-steel frame, which may have induced stresses in the sample during annealing.

When all of the experimentally controllable parameters were held constant, there was still a drift in the photon count rate of 0.02%/h. This drift was determined to arise either from the detector efficiency or from drifts in the detector electronics. Other possible artifacts such as air pressure changes or spectrometer motion were eliminated by careful tests. To correct for this drift, we normalized all of our data to measurements made on a "standard" sample of the same material. The standard sample was clamped to a second kinematic mount and was never annealed. The standard and the annealed sample were measured alternately approximately once an hour. The kinematic mounts insured that the samples were correctly repositioned. After each anneal a series of scans was collected for the sample and the standard. The integrated total of the diffracted counts $A$ and the integrated total of the transmitted counts $T$ were calculated after each scan by summing the counts at each point over all points in the scan. Each time the sample and the standard were switched, the diffracted and transmitted ratios were computed:

$$R(A)=A(\text{sample})/A(\text{standard}) ,$$
$$R(T)=T(\text{sample})/T(\text{standard}) . \quad (1)$$

The average of $R(A)$, defined as $\langle R_a \rangle_i$, and the average of $R(T)$, defined as $\langle R_t \rangle_i$, were then computed for each anneal (labeled by $i$), together with their standard deviations (see Table I). Changes in $\langle R_t \rangle$ with annealing were used to calculate the densification. Changes in $\langle R_a \rangle$ were used to rescale the data to compensate for drifts in the photon detection system; this is described in detail in Sec. III. For the actual number of switches between each anneal (5—18), the standard deviations of $\langle R_a \rangle$ and $\langle R_t \rangle$ were determined to be sufficiently small to achieve the desired precision (0.02—0.05 %).

Several checks ensured that the stability necessary for the required precision in the measured scattering intensity was maintained. The telemicroscope verified that the sample never moved more than 10 $\mu$m during any of the anneals. The centroid of the scattered intensity curve was monitored for each set of scans to confirm the absence of any beam motion (see Table I). To measure the stability between each pair of anneals, the first half of the set of sample scans taken between the two anneals were added together to form a composite sample scan, and a similar composite was formed from the second half. Before forming the composite scans, the individual scans were area normalized, i.e., scaled to have a common value for the total number of counts, to correct for the drift in the photon detection system. Then the first composite was subtracted from the second. The resulting difference was always a structureless envelope whose shape agreed with the expected Poisson noise. This verified the absence of any systematic shifts during the actual measurements of the sample scattering.

To check for long time drifts and for drifts during the time the sample was being annealed, composite standard scans were made by adding area-normalized scans of the standard taken between successive anneals of the sample. Since the standard was not annealed, its scattering should remain unchanged. To check for shifts across the anneal, the differences were taken between the composites before and after each anneal. The difference curves for the sample and for the standard before and after the first anneal of sample 1 are shown in Fig. 3(b). The measured sample change is clearly outside the noise indicated by the small change in the standard. The difference in the composite standard scan before and after this anneal is compared with the expected noise in Fig. 3(c). In all but one case, the difference in the standard before and after the anneal was consistent with statistics; shortly after the second anneal of the second sample, the beam apparently moved, causing the difference curve to resemble a first-derivative curve. A large change was also found in the position of the centroid of the sample scans before and after this anneal. For this reason, the difference curves for sample 2 between the first and second anneal could not be used.

## III. DENSIFICATION

The sample densification was determined from the changes in the transmission of the sample relative to the standard as a function of the anneals. This measurement of the density was necessary to correct the diffraction and resistance data, and proved to be of intrinsic interest as well. During each scan, the sample was rotated from $\phi=6.5°$ to $\phi=12.5°$. Assuming a homogeneous, flat sample, the sum of all the transmitted counts $T$ is given by

$$T=\sum_j I_0 \exp[-\mu t/\cos(\phi_j)] . \quad (2)$$

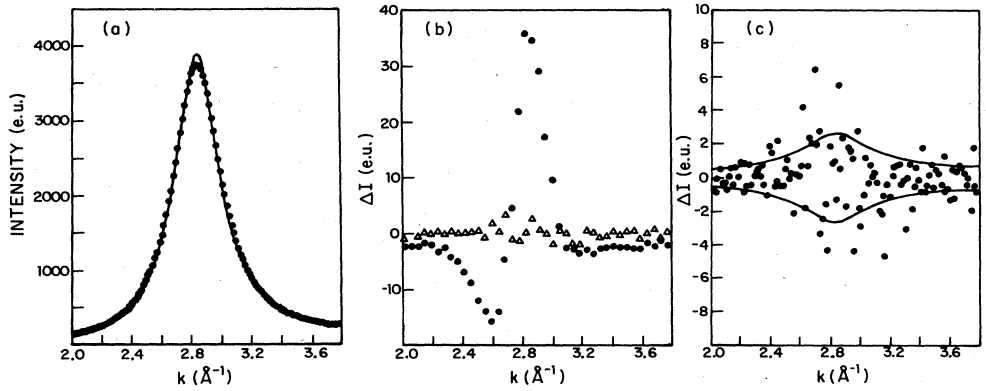


FIG. 3. (a) X-ray scattering intensity $I_{\text{e.u.}}(k)$ for the unannealed sample. The dots represent the data; the solid line represents the fit to the Percus-Yevick theory. The error bars are $<0.2\%$ for all points, and are $<0.05\%$ peak. All the intensities are given in electron units. (b) Comparison of the change in the x-ray scattering intensity of the sample and the standard before and after the first anneal of sample 1. The dots represent the difference in the scattering intensity between the unannealed sample and the sample annealed at 266 °C for 40 min. The triangles represent the difference in the scattering intensity measured for the standard before and after the anneal of the sample. Each sample scattering curve was a composite of 30 individual scans; each standard scattering curve was a composite of 17 scans interspersed with the sample scans. Every three data points have been averaged for clarity. (c) Comparison of the change in the standard before and after a sample anneal with the expected Poisson statistics. The dots represent the difference in the scattering measured for the standard before and after the first anneal of sample 1; each standard scan was a composite of 17 scans. The solid lines represent the expected standard deviation in the difference estimated from Poisson statistics: $\sigma=\sqrt{2N}$, where $N$ is the number of counts at $k$.

The sum is over all the points in the scan; $\mu$ is the absorption coefficient and $t$ is the sample thickness. $T$ depends on the density through the absorption coefficient since $\mu=(\mu/\rho)\rho$. Densification changes both the density and the sample thickness. The ratio of the sample transmission to the standard transmission after the $i$th anneal, $\langle R_t\rangle_i$, was calculated as described in the previous section. $\langle R_t\rangle_i$ is related to the value for the original unannealed sample by

$$\frac{\langle R_t\rangle_i}{\langle R_t\rangle_0}=\frac{T(\rho+d\rho_i)}{T(\rho)}\ , \tag{3}$$

where $d\rho_i$ is the change in density. Expanding $T$ for small $d\rho_i$ and recognizing that $d\rho_i/\rho=-\frac{1}{3}dt/t$ (assuming isotropic densification), the change in density is given by

$$\frac{d\rho_i}{\rho_0}=-\frac{3}{2}\frac{1}{\mu t}\left[\frac{\langle R_t\rangle_i}{\langle R_t\rangle_0}-1\right]\frac{T}{T'}\ , \tag{4a}$$

where

$$T'=\sum_j\left[\frac{-1}{\cos(\phi_j)}\right]\exp\left[\frac{-ut}{\cos(\phi_j)}\right]\ . \tag{4b}$$

For $\mu t$ between 1 and 2, and over the small angular range being considered here, $T/T'$ can be replaced by $-0.986$.

Values for $\mu t$ were determined by fitting the transmitted data to the form $I_0(\exp(-\mu t/\cos\phi))$; the values obtained from these fits are 1.57 for sample 1 and 1.13 for sample 2. These values are consistent with the measured thicknesses. The value for $\mu t$ calculated from the tabulated absorption coefficients for a 50-$\mu$m-thick sample is 1.22.[11] The value of the densification for each anneal is shown in Table I and Fig. 4. The resulting precision of 0.05% is as good as can be achieved by the best standard techniques. Typical errors for the density changes of glassy metals measured by other techniques are between 0.5 and 0.7%.[1]

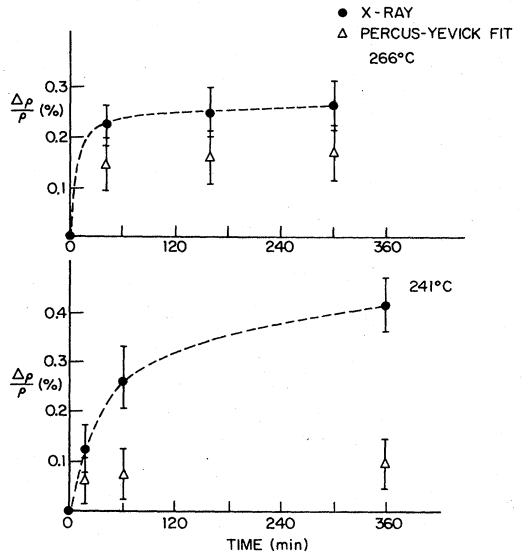


FIG. 4. Densification of amorphous $Pd_{82}Si_{18}$ as a function of isothermal annealing time. The annealing temperatures are indicated in the figure. The solid circles represent the measured densification values obtained directly from changes in the x-ray absorption. The triangles represent the densification values obtained by fitting the scattering intensity $I_{\text{e.u.}}(k)$ to a hard-sphere model derived from the Percus-Yevick theory. All the densification ratios are relative to the unannealed sample. The dashed line is a guide to the eye.

## IV. DATA ANALYSIS AND RESULTS

To compare the scattering intensities with minimum influence from the long term drifts in the detection system, all of the individual sample scans between the $i$th and the $(i+1)$th anneal were combined to form a composite scan, $I^i_{\text{comp}}(k)$, in the following way:

$$I^i_{\text{comp}}(k)=\frac{\langle R_a\rangle_i}{N_i}\sum_{j=1}^{N_i}\frac{I^i_j(k)}{A^i_j}\ . \tag{5}$$

$N_i$ is the number of sample scans taken between the $i$th and the $(i+1)$th anneal, $I^i_j(k)$ is the number of counts at scattering vector $k$ in the $j$th scan taken after the $i$th anneal, and $A^i_j$ is the total number of counts in this scan summed over $k$. Dividing $I^i_j(k)$ by $A^i_j$ gives the $j$th scan unit area. Multiplying by $\langle R_a\rangle_i$ normalizes the area of the composite scan to the area determined by the ratio of the sample to standard. A similar composite was created for the standard with the factor $\langle R_a\rangle_i$ set equal to 1. The area of the standard scans did not change since the standard was never annealed. For each point in the composite scan, the standard deviation was calculated from the sum of the individual area-normalized scans. This standard deviation was free of the systematic error associated with the drift in the detection system since the individual scans were scaled to have the same unit area before being added together. The calculated standard deviation was found to be consistent with the value expected from Poisson statistics.

Air scattering was measured to be approximately 5% of the sample scattering at $k=2.0$ Å$^{-1}$. Its contribution dropped off to less than 1% at $k=2.4$ Å$^{-1}$ and then became insignificant as the intensity rose steeply toward the peak at $k=2.84$ Å$^{-1}$. The measured air scattering, corrected for the sample absorption, was subtracted from the sample scattering. Polarization by the sample and the monochromators was also accounted for in the standard way,[12] by a factor of $1+\cos^2(2\theta)\cos^4(2\theta_M)$ where $2\theta_M$ is the scattering angle in the monochromator and analyzer.

In the transmission geometry, the attenuation factor for absorption in the sample is $[\rho t/\cos(\phi)]\exp[-\mu t/\cos(\phi)]$. The small changes in sample density after each anneal add a correction to the absorption factor which is proportional to the densification. The corrected scattering after the $i$th anneal $I^i_{\text{corr}}(k)$ is related to the observed scattering $I^i_{\text{comp}}(k)$ by

$$I^i_{\text{corr}}(k)=I^i_{\text{comp}}(k)\left[1-\frac{2}{3}\frac{d\rho_i}{\rho}\left[1-\frac{\mu t}{\cos(\phi)}\right]\right]\times\frac{\cos(\phi)}{\mu t}\exp\left[\frac{\mu t}{\cos(\phi)}\right]\ , \tag{6}$$

where $\mu t$ and $\rho$ are measured on the unannealed sample and $d\rho_i$ is the change in density. The measured value for the densification was used to make this correction.

The measured intensity was converted to electron units (e.u.) in two ways. The volume of air responsible for the air scattering was estimated from the measured angular divergence of the monochromator and the analyzer. Scaling the measured air scattering to agree with the expected values calculated from the atomic form factors (assuming a composition of 80% nitrogen and 20% oxygen) allowed us to convert the measured air scattering intensity into electron units; applying the resulting conversion factor to the $Pd_{82}Si_{18}$ data resulted in a peak height of 3600 e.u. Alternatively, the $Pd_{82}Si_{18}$ data at high angles was compared with the expected values from the Pd and Si form factors, resulting in a peak height of 3900 e.u. The average of these values, 3750 e.u., was chosen for scaling the measured data. These estimates compare favorably with the previously measured values of 3350 (Ref. 13) and 3700,[10] for the similar system $Pd_{80}Si_{20}$.

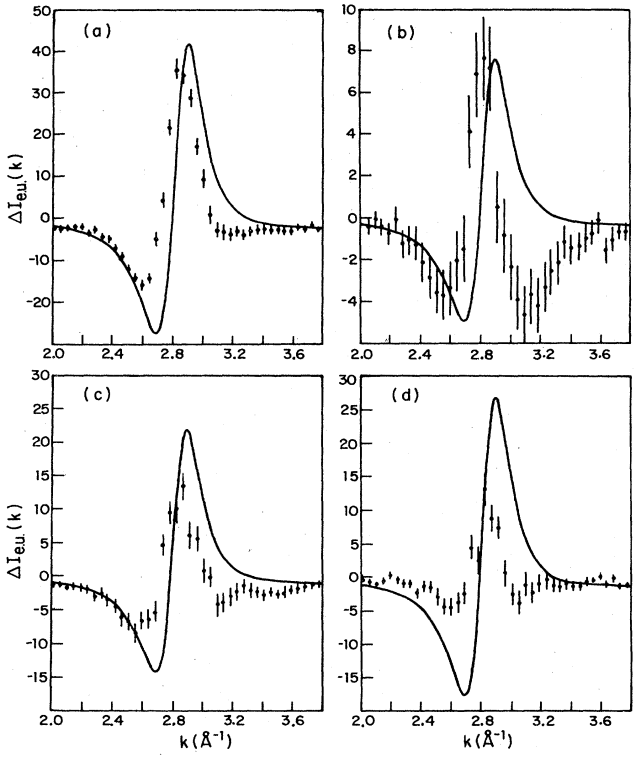


FIG. 5. Difference in the x-ray scattering intensity $\Delta I_{e.u.}(k)$ versus $k$ between successive anneals. The dots represent the data; the solid line represents the fit to the Percus-Yevick theory. All the intensities are in electron units; three data points have been averaged for clarity. (a) Difference between scattered intensity from sample 1 after 40-min anneal at 266 °C and that from the unannealed sample 1. (b) Difference between scattered intensity from sample 1 after total anneal of 5 h at 266 °C and that from sample 1 after 40 min at 266 °C. (c) Difference between scattered intensity from sample 2 after 15-min anneal at 241 °C and that from the unannealed sample 2. (d) Difference between scattered intensity from sample 2 after total anneal of 6 h at 241 °C and that from sample 2 after 1 h at 241 °C.

The x-ray scattering intensity $I_{e.u.}(k)$ in electron units is shown in Fig. 3(a). The smooth line represents a fit to a Percus-Yevick hard-sphere model which is discussed in the next section. The scattering curve becomes narrower and its peak becomes higher with each anneal. Table I lists the changes in the height of the peak and in its width (parametrized by the second moment of the curve).

The change in the scattering curves with annealing is small, and is most clearly shown by computing the difference in the scattering before and after the anneal. These difference curves are shown in Fig. 5. For sample 1, it is clear that most of the change occurred during the first anneal. This anneal resulted in the greatest density change, and the difference curve clearly shows the greatest change although it still has only a 1% change in the peak height; the error in the intensity of the peak is only 0.05%. Several features of this difference curve are particularly noteworthy: the large negative change on the low-$k$ side of the peak, the positive change in peak height, and the absence of any significant change on the high-$k$ side of the peak. This contrasts with the best previous experiments done on $Pd_{80}Si_{20}$ by Waseda and Egami,[10] who find little change on the low-$k$ side of the first peak and a large change on the high-$k$ side. The changes we observed after the second and third anneals of the first sample were smaller, so they are shown added together. The resulting difference curve appears slightly different from the first anneal, with a larger change on the high-$k$ side of the peak making the difference curve more symmetric.

For the second sample, the zeroth-to-first anneal difference has very much the same shape as that for the first sample. The smaller magnitude which is observed is consistent with the smaller densification. The first-to-second anneal is not shown because of the beam motion discussed earlier. The second-to-third anneal seems to have slightly greater change on the high-$k$ side of the peak than the zeroth-to-first, but otherwise has a similar shape to the first anneal difference curve.

## V. PERCUS-YEVICK MODEL

The shape of the difference curves results from a combination of a narrowing of the peak and a shift in its position. These changes can be understood from the structural relaxation. In real space, the free volume decreases as the atomic packing becomes denser. The probability distribution of particles at a distance $r$ from a given particle, will show an increase at the second-nearest-neighbor and higher-order-neighbor positions. The resulting broader envelope in real space, arising from this growth at the higher-order positions corresponds to a sharpening of the first peak in $k$ space. The small shift of the peak to higher $k$ corresponds to the tighter packing in the relaxed glass.

To obtain an analytic expression for the differences curves, we used a simple model for the structure, the Percus-Yevick theory.[3] When a hard-sphere potential is used, an analytic expression for the structure factor as a function of the hard-sphere diameters $R_1$ and $R_2$ and the density $\rho$ is obtained. We used the solution for the two-

component hard-sphere potential derived by Lebowitz[14] with the computational simplification suggested by Weeks.[15] Quantitative agreement was not expected from such a simple theory, but it was hoped that the qualitative features of the difference curves could be shown to arise directly from the densification. The Percus-Yevick theory has the advantage over all finite-size model calculations of not being limited by the size of the model. This is of particular importance for the details of the first diffraction peak which are of interest here.

The theoretical expressions for the partial structure factors $S_{\alpha\beta}$ were converted to a scattering intensity by multiplying by the appropriate form factors:[16]

$$I_{\rho y}(k)=s'\left[\sum_{\alpha,\beta}(c_\alpha c_\beta)^{1/2}S_{\alpha\beta}(k)f_\alpha f_\beta\right]. \tag{7}$$

The $c_\alpha$ and $c_\beta$ are the concentrations of the atomic species; $s'$ is a scaling factor which should be equal to 1.0 if the measured electron unit scaling factor was chosen correctly. The x-ray data was fit to this form by a nonlinear least-squares fitting routine based on the Marquardt algorithm.[17] The data was combined so that a single set of parameters $R_1$, $R_2$, and $s'$ was chosen to optimize the fit over the different anneals. The only parameter allowed to vary (as a function of the anneal) was the density. For sample 1, all four anneals were fit with the same $R_1$, $R_2$, and $s'$. For sample 2, all the data before the beam motion were fit separately from the data after. The results obtained from the fitting are shown in Table II. The values obtained for the scaling factors are very close to 1.0. In fact, the error in $s'$ from the fits is less than what one would expect from the known errors in the absorption coefficients, so the values of $s'$ confirm the original factor is consistent with the conversion to electron units.

The measured density of $Pd_{82}Si_{18}$ is 10.6 g/cm$^3$,[10] which corresponds to an average atomic volume of $1.46\times10^{-23}$ cm$^3$. The fit value for the density corresponds to an atomic volume of $1.39\times10^{-23}$ cm$^3$. The change in the density predicted by the Percus-Yevick analysis that gives the best fit to the data is shown in Fig. 4 for comparison with the measured densification. The predicted value of the density change is consistently low, but the trend in the data is qualitatively correct. For the second sample, the result for the last anneal at 241 °C was obtained separately from the first two anneals because of the beam motion. This result was added to the extremely low value for the second anneal of sample 2 to get the total densification.

TABLE II. Results of fitting Eq. (7) to Percus-Yevick form.

| Anneal | $\rho_i$ ($10^{23}$/cm$^3$) | $d\rho_i/\rho_0$ (%) |
|---|---|---|
| | Sample 1 | |
| | $R_1=2.6046$, $R_2=1.5538$, $s'=1.0048$ | |
| unannealed | 0.723 65±0.000 02 | 0 |
| 1 | 0.724 68 | 0.145 |
| 2 | 0.724 77 | 0.155 |
| 3 | 0.724 82 | 0.162 |
| | Sample 2 | |
| Before beam motion | | |
| | $R_1=2.6048$, $R_2=1.5377$, $s'=0.9981$ | |
| unannealed | 0.724 93 | 0 |
| 1 | 0.725 40 | 0.064 |
| 2 | 0.725 44 | 0.073 |
| After beam motion | | |
| | $R_1=2.6060$, $R_2=1.5372$, $s'=0.9968$ | |
| 2 | 0.725 00 | 0 |
| 3 | 0.725 21 | 0.030 |

The quality of the fit to the data can be seen in Fig. 3(a). The peak of the fit is overly high, and the centroid is at slightly higher $k$ than the real data. This problem has been addressed by Weeks,[15] who attributes it to the use of a hard-core potential. A soft-core potential would move the peak to lower $k$ and decrease the peak height. Both of these changes would improve the fit. Unfortunately, there is no simple analytic solution for a soft-core potential.

The difference curves generated by the Percus-Yevick theory are shown in Fig. 5. The curves were obtained by changing the density according to the measured values of the densification, while keeping all the other parameters constant. Using the density changes obtained directly from the Percus-Yevick fits does not significantly improve the agreement with the measured difference curves. All the Percus-Yevick difference curves show the same features: the asymmetry resulting from the peak narrowing and shifting, a large negative change on the low-$k$ side of the peak, a large positive change in the peak height, and a small change on the high-$k$ side of the peak. This predicted shape agrees with the data best for the anneal of sample 1, which had the largest single density change. It does not agree well with the later anneals on sample 1 where the density changes and the corresponding scattering intensity changes are much smaller. The shape of the difference curves for sample 2 after both anneals is more symmetric than that for the first anneal of sample 1 and consequently the fit to the Percus-Yevick difference is somewhat poorer. In all cases, the change in peak height with density for the Percus-Yevick form is reasonable. Since the measured densification of the sample was used for the model, one must look to other factors to account for the disagreement between the fit and the data. It is possible that structural factors that are not accounted for by the Percus-Yevick model, such as chemical short-range order, must be taken into account.

## VI. RESISTIVITY MEASUREMENT

The original motivation for the present experiment came from studies of the change in the resistivity of amorphous metals with annealing.[6] Simple theories of resistivity in liquid metals treat the conduction electrons as nearly free electrons propagating through the weakly scattering liquid structure. Scattering by the ion cores keeps the electrons from propagating indefinitely and leads to the finite conductivity. In amorphous metals, the liquidlike structure is frozen in; the relaxation of the structure induced by annealing changes the scattering properties and gives rise to the observed changes in the x-ray scattering. The mean scattering length of the conduc-

tion electrons (i.e., the average distance an electron travels before colliding with an ion) changes, leading to a change in the resistivity. Although the scattering strength is different for the electrons and the x-rays, by estimating the atomic pseudopotential $v(k)$ which the electrons scatter from, and then scaling this to the electron density, which the x-rays scatter from, we can estimate the electrical resistivity from the x-ray scattering intensity.

The general expression for x-ray scattering from an amorphous material is

$$I(\mathbf{k})=\sum_{i,j}\exp(i\mathbf{k}\cdot\mathbf{r}_{ij})f_i(\mathbf{k})f_j(\mathbf{k})\ , \tag{8a}$$

where $f_i(\mathbf{k})$ is the form factor for the $i$th atom and $\mathbf{r}_{ij}$ is the vector between the $i$th and $j$th atoms. The sum is over all atoms and

$$f(\mathbf{k})=\int\exp(i\mathbf{k}\cdot\mathbf{r})n_i(\mathbf{r})d\mathbf{r}\ , \tag{8b}$$

where $n_i(\mathbf{r})$ is the electron density of the $i$th atom. The basis of the Ziman theory is a similar scattering process which occurs for the conduction electrons in metals. Several sources give detailed derivations of the Ziman theory,[4,18] so only a sketch is presented here. For materials which are nearly-free-electron-like, the wave function of the conduction electron $|k\rangle$ is taken to be a free electron wave. The probability of scattering from one state on the Fermi surface to another is given by

$$Q(\theta)=V_0\frac{2\pi}{\hbar}|\langle k|V|k'\rangle|^2\frac{N(E_F)}{(8\pi)}\ , \tag{9}$$

where $N(E_F)$ is the density of states per unit volume at the Fermi energy, $V$ is the potential, and $V_0$ is the atomic volume.

The resistivity is related to the scattering probability by

$$\rho_e=3\frac{m^2}{(e\hbar k_F)^2}\frac{1}{N(E_F)}\int(1-\cos\theta)Q(\theta)d\Omega\ . \tag{10}$$

Substituting the matrix element for $Q(\theta)$ and changing the angular integration to an integration over $k$ leads to

$$\rho_e=\frac{3m^2V_0}{(e\hbar k_F)^2}\frac{4\pi}{\hbar}\int_0^1|\langle k|V|k'\rangle|^2\left[\frac{k}{2k_F}\right]^3 d\left[\frac{k}{2k_F}\right]\ . \tag{11}$$

In the nearly-free-electron model, the matrix element squared is

$$|\langle k|V|k'\rangle|^2=\sum_{i,j}\exp[i(\mathbf{k}\cdot\mathbf{r}_{ij})]v_i(\mathbf{k})v_j(\mathbf{k})\ . \tag{12}$$

The scattering between the expression for the x-ray scattering, Eq. (8), and the expression for the resistivity is clear; the difference is the replacement of the x-ray form factors by the pseudopotential $v(k)$.

In deriving the pseudopotential, the full Coulomb potential is replaced by a weaker potential created by the screening electrons. The relation between the screening electron charge density in $k$ space, $n_{sc}(k)$, and the pseudopotential $v(k)$ is given by the Lindhard screening expression:

$$n_{sc}(k)=F(k)v(k)\ , \tag{13a}$$

with

$$F(k)=\frac{-mk_F}{(\pi\hbar)^2}\left[\frac{1}{2}+\frac{1-(k/2k_F)^2}{4(k/2k_F)}\right]\ln\left[\frac{1+(k/2k_F)}{1-(k/2k_F)}\right]\ . \tag{13b}$$

The screening charge density is not the same as the full atomic electron density. This can be seen by comparing the asymptotic behavior of the two expressions. At $k=0$, the value of the atomic form factor goes to $z$, the number of electrons in the atom. The value of the screening density at $k=0$ is $n_{sc}(k=0)=k_F^3/3\pi^2=z^*/V_0$.

Using the measurement of Mizutani and Massalski[19] of the Fermi level ($2k_F=2.41$ Å$^{-1}$) and an atomic volume of $V_0=1.5\times10^{-23}$ cm$^3$, we find that $z^*=0.88$. We approximate $n_{sc}(k)$ by using the full electron density $f(k)$ multiplied by $(z^*/\langle z\rangle)$ to give it the proper value at $k=0$. Since the density of the screening electron is spread out further in real space than the atomic electron density, $n_{sc}(k)$ will drop off faster in $k$ space than $(z^*/\langle z\rangle)f(k)$. Consequently, this estimate of $n_{sc}(k)$ is an overestimate and the predicted resistivity will be larger than the actual resistivity.

Substituting $v(k)=f(k)(z^*/\langle z\rangle)[1/(V_0F(k)]$ into the expression for the matrix element gives

$$|\langle k|v|k'\rangle|^2=\left[\frac{z^*}{\langle z\rangle V_0F(k)}\right]^2 I_{\text{e.u.}}(k)\ , \tag{14}$$

where $I_{\text{e.u.}}(k)$ is the intensity of x-ray scattering.

The estimate for the resistivity in terms of the x-ray scattering now becomes

$$\rho_e=\left[\frac{z^*}{\langle z\rangle}\right]^2\left[\frac{12\pi^5\hbar}{e^2k_F^4V_0}\right]\int_0^1\frac{I_{\text{e.u.}}(k)}{G(x)}x^3dx\ , \tag{15a}$$

where $x=k/2k_F$ and

$$G(x)=\frac{1}{2}+\frac{1-x^2}{4x}\ln\left[\frac{1+x}{1-x}\right]\ . \tag{15b}$$

Using $V_0=1.5\times10^{-23}$ cm$^3$ and $k_F=1.2\times10^8$/cm, this becomes

$$\rho_e=[2.25\ (\mu\Omega\,\text{cm})]\int_0^1\frac{I_{\text{e.u.}}}{G(x)}x^3dx\ . \tag{16}$$

Evaluating the integral gives a value for the resistivity equal to 279 $\mu\Omega$ cm. The quoted error for the measurement of $2k_F$ is $2k_F=2.41\pm0.08$. This leads to an error in the estimate of the resistivity, so $\rho_e=279\pm82$ $\mu\Omega$ cm. This should be compared with experimentally obtained values of 74 $\mu\Omega$ cm.[20] As expected, the x-ray result overestimates the resistivity. However, it is important to note that there are no free parameters in this evaluation since all the quantities that go into the estimate of the resistivity were experimentally determined. The agreement to within an order of magnitude for the absolute value of the resistivity is quite satisfactory for such a crude model.

We expect better agreement for a calculation of the relative changes in resistivity than for the absolute resistivity for two reasons: (i) Dividing the calculated change in the

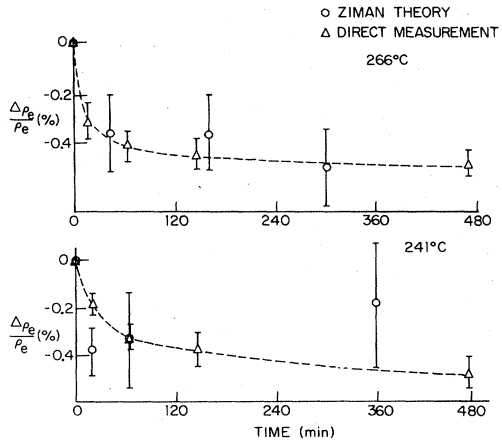


FIG. 6. Percent change in resistivity ($d\rho/\rho$) versus isothermal annealing time. The solid circles represent the ratios calculated from the Ziman theory using the x-ray data. The triangles represent four-point probe ac bridge measurements corrected for the sample densification. The dashed line is a guide to the eye.

resistivity by the calculated resistivity cancels out the effect of any incorrect prefactors or normalization errors; and (ii) the integral for the calculation of the resistivity is heavily weighted toward the region near $2k_F$ [by the $x^3$ in the integrand and the rising of $S(k)$ toward the first peak] which lessens the effect of the shape of the pseudopotential on the integral. Since the pseudopotential is not expected to change significantly with annealing, an incorrect form for the pseudopotential is much less serious for calculating the relative changes in the resistivity than for the absolute resistivity. The large change in $S(k)$ from $k=2.0$ to $2k_F$ and the change in the Fermi level with densification account for over 85% of the resistivity change.

In order to estimate the change in resistivity with annealing, it is necessary to take into account the effect of density changes since the upper limit on the integral is $2k_F$. As the sample densifies, the Fermi level is not constant; $dk_F/k_F=\frac{1}{3}d\rho/\rho$ in the nearly-free-electron approximation. Taking this effect into account, the changes in resistivity were calculated from Eq. (15a) and are shown in Table I; the changes in the Fermi level used for the calculation are also shown for each case. The large error bars on the resistivity changes do not result from the uncertainty in the integral, but arise from the uncertainty in the change in the Fermi level.

The resistivity changes measured by the ac technique are compared with the results of the Ziman theory in Fig. 6. The measured resistance changes have been corrected for sample densification to yield resistivity changes. The good agreement provides strong evidence that the change in resistivity is induced by structural change, and that the Ziman theory is adequate for explaining these changes in this alloy.

## VII. CONCLUSION

The major result of this work has been the high-precision measurement of the x-ray scattering by amorphous $Pd_{82}Si_{18}$, and the change in scattering caused by structural relaxation. We have taken great care to minimize systematic errors so that the small changes in $S(k)$ with isothermal annealing could be measured accurately. By using several methods to maintain the system stability, we obtained a reliable measurement of $S(k)$ and the error associated with this measurement. To correct for drift in the detectors, two samples were used, one to anneal and the other to recalibrate the spectrometer. Other spectrometer parameters such as sample position, beam position, and beam intensity were carefully monitored. The change in the scattering curve for the unannealed sample determined the precision of our measurement. Previous measurements of structural relaxation may have suffered from some of these problems; no previous work has addressed all of them directly.

Simultaneously, with the scattering measurements, x-ray absorption measurements of the densification were made with a precision equal to that of immersion techniques. The measured changes in the density were crucial to the Ziman theory calculation of the resistivity changes because of the resulting shift in the Fermi level. The magnitude of the observed densification was significant; it must be included as an absorption correction for the x-ray scattering, and to obtain the proper resistivity changes from the measured resistances.

Using the Percus-Yevick theory, the x-ray scattering intensity was fit to a two-component hard-sphere model. Some of the apparent differences between the measured scattering curve and the theoretical curve may be explained by the failure of the hard-sphere potential to properly describe the real atomic potential. The measured changes in the density were used to model the changes in $S(k)$. The Percus-Yevick difference curves all showed the same features, corresponding to a sharpening of the peak and a shift in its position to higher $k$. The measured x-ray difference curves agree with this shape for the first anneal of each sample, but are more symmetric for the later anneals.

We used the Ziman theory to compare the measured changes in $S(k)$ with the changes in the electrical resistivity measured for each sample. Previous comparisons of the Ziman theory with experiment have depended heavily on the calculation of the pseudopotential. By concentrating primarily on changes in the resistivity rather than the absolute resistivity, we emphasize the part of the Ziman theory that is structure dependent and experimentally more accessible. A simple approximation allowed us to calculate the absolute resistivity and resistivity changes without calculating the atomic pseudopotential. This approximation gave a reasonable estimate of the absolute resistivity and a good estimate of the relative changes in the resistivity.

## ACKNOWLEDGMENTS

We thank W. L. Johnson (Caltech) for providing the samples and Frank Molea for assistance with the x-ray generator. This work was supported by the Materials Research Laboratory under National Science Foundation Contract No. NSF-DMR80-20247 and by the Office for Naval Research Contract No. N00014-77-C-0002.

*Present address: Department of Metallurgy and Materials Science, University of Cambridge, Cambridge CB2 3QZ, U.K.

†Present address: Department of Physics, Washington University, St. Louis, MO 63130.

‡Present address: Department of Physics, University of Washington, Seattle, WA 98195.

§Present address: Department of Physics, University of Texas, Arlington, TX 76019.

[1]G. S. Cargill III, in *Solid State Physics*, edited by H. Ehrenreich, F. Seitz, and D. Turnbull (Academic, New York, 1975), p. 227.

[2]A. L. Greer, J. Non-Cryst. Solids, **62**, 737 (1984).

[3]J. K. Percus and G. J. Yevick, Phys. Rev. **110**, 1 (1958).

[4]J. M. Ziman, Philos. Mag. **6**, 1013 (1961); T. E. Faber and J. M. Ziman, *ibid.* **11**, 153 (1965).

[5]E. Esposito, H. Ehrenreich, and C. D. Gelatt, Phys. Rev. B **18**, 3913 (1978).

[6]K. F. Kelton and F. Spaepen, in *Proceedings of the 4th International Conference on Rapidly Quenched Metals,* edited by T. Masumoto and K. Suzuki (Japanese Institute of Metals, Sendai, 1982), p. 527.

[7]C. P. Chou and D. Turnbull, J. Non-Cryst. Solids **17**, 169 (1975).

[8]A more complete description of the triple-axis spectrometer can be found in J. Collett, Ph.D. thesis, Harvard University (1983); J. Als-Nielsen, J. D. Litster, R. J. Birgeneau, M. Kaplan, C. R. Safinya, A. Lindegaard-Andersen, and S. Mathiesen, Phys. Rev. B, **22**, 312 (1980).

[9]B. D. Cullity, *Elements of X-Ray Diffraction* (Reading, Addison-Wesley, 1969).

[10]Y. Waseda and T. Egami, J. Mater. Sci., **14**, 1249 (1979).

[11]*International Tables for X-Ray Crystallography* (Kynoch, Birmingham, 1970), Vol. III.

[12]B. E. Warren, *X-Ray Diffraction* (Reading, Addison-Wesley, 1969).

[13]P. Mrafko and P. Duhaj, Phys. Status Solidi A **22**, 151 (1974).

[14]J. L. Lebowitz, Phys. Rev. **133**, 895 (1964).

[15]J. D. Weeks, Philos. Mag. **35**, 1345 (1977).

[16]N. W. Ashcroft and D. C. Langreth, Phys. Rev. **156**, 685 (1967).

[17]D. A. Marquardt, J. Soc. Ind. Appl. Math. **11**, 431 (1963).

[18]G. Busch and H. J. Guntherodt, in *Solid State Physics,* edited by H. Ehrenreich, F. Seitz, and D. Turnbull (Academic, New York, 1974).

[19]U. Mizutani and T. B. Massalski, Phys. Rev. B **21**, 3180 (1980).

[20]K. F. Kelton and F. Spaepen, Phys. Rev. B **30**, 5516 (1984).